RSC Advances

PAPER

View Article Online
View Journal | View Issue

Cite this: *RSC Adv.*, 2021, **11**, 4221

Can a gas phase contact ion pair containing a hydrocarbon carbocation be formed in the ground state?†

José R. Araújo,[a] Railton B. de Andrade,[a] Hélcio J. Batista,[b] Elizete Ventura[a] and Silmar A. do Monte*[a]

Received 14th December 2020
Accepted 11th January 2021

DOI: 10.1039/d0ra10523f

rsc.li/rsc-advances

So far, no conclusive evidence of a ground-state contact ion-pair containing a hydrocarbon carbocation has been given in the gas phase. Due to the very high stability of the 1,2:4,5-dibenzotropylium (or dibenzo[*a*,*d*]tropylium) carbocation, we suggest (supported by DFT and MP2 calculations) the formation of a contact ion pair between this carbocation and chloride, occurring during the reaction between 1,2:4,5-dibenzotropyl (also named dibenzo[*a*,*d*]tropyl or dibenzo[*a*,*d*]cycloheptenyl) radical and chlorine atom at very low temperatures, through the harpoon mechanism. This is the first modeling study to find computational evidence for the possibility of a gas-phase contact ion pair (containing a hydrocarbon carbocation) formed in the ground state. Identification of this metastable species can be carried out by trapping it in He nanodroplets, along with infrared laser spectroscopy routinely coupled with this technique.

Introduction

Since the 1950s, the concept of ion pairs has been widely used to explain the observed kinetic behavior of ground-state reactions in the gas phase.[1–25] Among these examples, one can highlight two for which intimate (or contact) ion-pairs are characterized as intermediates (that is, as stable species) through density functional theory (DFT) calculations.[22,24] In both cases, the cation unit of the ion-pair contains at least one heteroatom. Other examples of stable ground state contact ion-pairs in the gas phase are found in the molecules of ionic liquids,[26–46] whose cations also contain at least one heteroatom. A common feature of these ion pairs is the occurrence of hydrogen bond(s) between the opposite ions.[22,24,26–46] Thus, they can be named hydrogen-bonded contact ion pairs (HBCIP).

Our group recently reported, through the use of highly correlated multi-reference configuration interaction calculations, several examples of gas-phase contact ion pairs formed in excited states.[47–50] Three of these four examples are HBCIP,[47,49,50] and two of them contain hydrocarbon carbocations, $[CH_3]^+$ (ref. 47) and $[C_2H_5]^+$.[50] According to Hunt *et al.*,[44] the H bond in the $[CH_3]^+Cl^-$,[47] $[CF_3CH_2]^+Cl^-$ (ref. 49) and $[C_2H_5]^+Cl^-$ (ref. 50) ion pairs should be classified as doubly ionic H-bonds.

From what has been said, the following question arises: is it possible to have a ground-state HBCIP whose carbocation is a hydrocarbon? The motivation for this possibility came from Morton's work,[9] in which the author shows hypothetical potential energy curves for gas-phase reaction between *tert*-butyl cation and bromide and for gas-phase HBr elimination from neopentyl bromide. In these curves, the author suggests very shallow minima corresponding to HBCIP, with very low barriers, and in both cases, the carbocation is a hydrocarbon.

In addition to the partial recovery of the dissociative heterolysis energy by the coulombic attraction in the HBCIP, it is clear from the previous examples that an H bond's presence is an essential characteristic for the stabilization of many intimate ion pairs. Besides, from some examples studied by our group, the C^+–H···Cl^- moiety is associated with high binding energies.[47,49,50] Thus, if one can combine the presence of this moiety with a very stable carbocation able to form more than one H bond with the anion, one can have, in principle, a stable (that is, a minimum) ground-state ion pair containing a hydrocarbon carbocation. Good candidates are aromatic carbocations, such as derivatives of the tropilidene unit like tropylium cation[51] and its fused-ring aromatic derivatives containing at least one benzene ring, like the well-known benzotropylium[52–57] and dibenzotropylium[52,55,58,59] cations. The main idea to be explored is that additional benzene rings in resonance with the tropylium cation should increase the carbocation stability.

In the work of Hjelmencrantz *et al.*,[60] the NMR spectrum of a chlorine-substituted dibenzotropilidene unit (R), namely 5-chloro-5*H*-dibenzo[*a*,*d*]cycloheptene, is studied in toluene at several temperatures, allowing identification of two covalent isomers. Although an equilibrium between a covalent form and

[a]*Departamento de Química, CCEN, Universidade Federal da Paraíba, João Pessoa, PB, 58059-900, Brazil. E-mail: silmar@quimica.ufpb.br*

[b]*Departamento de Química, Universidade Federal Rural de Pernambuco, Recife, PE, 52171-900, Brazil*

† Electronic supplementary information (ESI) available. See DOI: 10.1039/d0ra10523f

a contact ion pair is also possible, the authors did not identify any signal consistent with the dibenzo[*a*,*d*]tropylium cation, even at the lowest temperature (−80 °C) employed. One possible explanation is that the conversion from the ion pair to the covalent form is fast on the NMR-time scale, which precludes the detection of the contact ion pair by this technique.[60] Besides, as the free energy of the ion pair is much higher than that of the covalent form, as will be discussed later, the equilibrium concentration of the former is much smaller than that of the latter, which imposes an additional difficulty for the contact ion pair detection.

In this work, we suggest, supported by Møller–Plesset perturbation theory to the second-order (MP2) and DFT calculations, the formation of a contact ion pair, [R^+Cl^-], between the dibenzo[*a*,*d*]tropylium cation (R^+) and chloride anion in the gas phase, occurring during the reaction between 1,2:4,5-dibenzotropyl (also named dibenzo[*a*,*d*]tropyl or dibenzo[*a*,*d*]cycloheptenyl) radical ($R^\bullet$) and chlorine atom ($Cl^\bullet$) at very low temperatures, through the harpoon mechanism. Furthermore, the HBCIP channel competes with the covalent (R–Cl) one. The HBCIP studied here corresponds to the first modeling study to find computational evidence for the possibility of a stable gas-phase ground-state ion pair containing a hydrocarbon carbocation. Its possible detection through trapping in He nanodroplets (HND) is also discussed. This technique is very well suited to isolate and detect metastable species and also allows pickup of open-shell species with minimum internal and translational energies, a proper condition to yield the mentioned HBCIP, as discussed later.

Computational details

Full geometry optimizations have been performed for the two covalent isomers of the 5-chloro-5*H*-dibenzo[*a*,*d*]cycloheptene (R–Cl, where R = dibenzotropylium), named cov1 and cov2, for the ion pair (R^+Cl^-) and the two transition states (TS1 and TS2), at the DFT and MP2 levels. One transition state (TS1) connects the ion pair to one of the covalent forms (cov1, see Fig. 1), while the other connects the two covalent forms (TS2, see Fig. 1). The connectivities of both TS1 and TS2 were found by moving the TS along the imaginary frequency mode (in both directions), followed by a visual inspection and reoptimization of the obtained structure. The chosen functional was M05-2X,[61] based on its excellent performance for calculating ion-pair binding energies of pyrrolidinium-based ionic liquids.[62] As analytical gradients are not available at the restricted open-shell MP2 (ROMP2) level and as spin contamination at the spin unrestricted MP2 (UMP2) level is considerably high for the dibenzo[*a*,*d*]tropyl radical ($R^\bullet$), optimization of $R^\bullet$ has only been performed at the restricted open-shell M05-2X (ROM05-2X) level. In this case, the reported results at the ROMP2 level correspond to single-point calculations performed on the geometry optimized at the DFT level. For the sake of consistency, this approach has also been applied for the dibenzo[*a*,*d*]tropylium cation (R^+), but at the RMP2 level.

To compute the relative equilibrium concentrations of the covalent and ion pair systems in toluene, calculations using the CPCM polarizable conductor continuum solvent model[63,64] have also been performed at the DFT level.

Normal mode analysis has been performed for all optimized structures to confirm whether they are minima or TS. With the exception of the CPCM calculations (for which a temperature of 193 K (−80 °C) has been used), all thermochemical calculations have been performed at 0.4 K (the approximate temperature of helium nanodroplets). C_s symmetry has been imposed for the transition states and for the covalent structures, while for $R^\bullet$ and R^+, C_{2v} symmetry has been used. For the HBCIP, C_s and C_{2v} symmetries have been used at the MP2 and DFT levels, respectively. The basis set superposition error (BSSE) has been taken into account for the HBCIP and for TS1 (see Fig. 1), through the counterpoise method[65] incorporated into the geometry optimization and frequency calculations.[66] 6-31++G**,[67–70] the mixed 6-311++G**(Cl,H)/6-31++G**(C), and the 6-311++G** basis sets[71,72] have been used at the DFT level, while at the MP2 level, only the first two basis sets have been used. All calculations have been performed with the Gaussian 09 software using its default setup.[73]

In order to characterize the excited charge-transfer state associated with the back electron transfer (step 3 of the suggested mechanism, as explained below), time-dependent (TD) CAM-B3LYP[74,75] calculations have been performed with the 6-31++G**, the mixed 6-311++G**(Cl,H)/6-31++G**(C),and the 6-311++G** basis sets. This functional has been chosen based on its good description of charge-transfer states in several systems.[76–78]

Results and discussion

Fig. 1 shows the qualitative gas-phase relative energies between the studied structures and dissociation channels. The assumed reaction profiles are also indicated. The ionic dissociation channel is shown for comparison. As no TS connecting the second covalent structure (cov2) to HBCIP has been found, it is assumed that there is no direct pathway for the interconversion between HBCIP and cov2. k_1, k_2, and k_3 are the rate constants for the $R^\bullet + Cl^\bullet \rightarrow$ cov1, $R^\bullet + Cl^\bullet \rightarrow$ HBCIP, and HBCIP $\rightarrow$ cov1 reactions, respectively.

In Table 1, the computed relative gas-phase free energies (ΔG) between the studied structures are given, including the neutral ($R^\bullet + Cl^\bullet$) and the ionic channels ($R^+ + Cl^-$). Although C_s symmetry has been imposed at the MP2 level, all results obtained for HBCIP at this level lead to structures with almost C_{2v} symmetry. The Cartesian coordinates of all optimized structures are given in the ESI.†

As can be seen from Table 1, the largest variations of the ΔG values are observed for HBCIP and TS1 with BSSE, changing by at most ∼14 kcal mol^{-1} (as the method changes, with the 6-31++G**(H,Cl)/6-31++G**(C) basis set). The corresponding maximum change without BSSE is ∼8 kcal mol^{-1}. At a given level (DFT or MP2), the ΔG values vary at most ∼2 kcal mol^{-1}. Thus, the effect of the method is more relevant than the effect of the basis set. The BSSE effect is much larger at the MP2 level, changing the ΔG values of the HBCIP by 5.68 and 6.31 kcal mol^{-1}, and those of TS1 by 5.89 and 6.73 kcal mol^{-1},

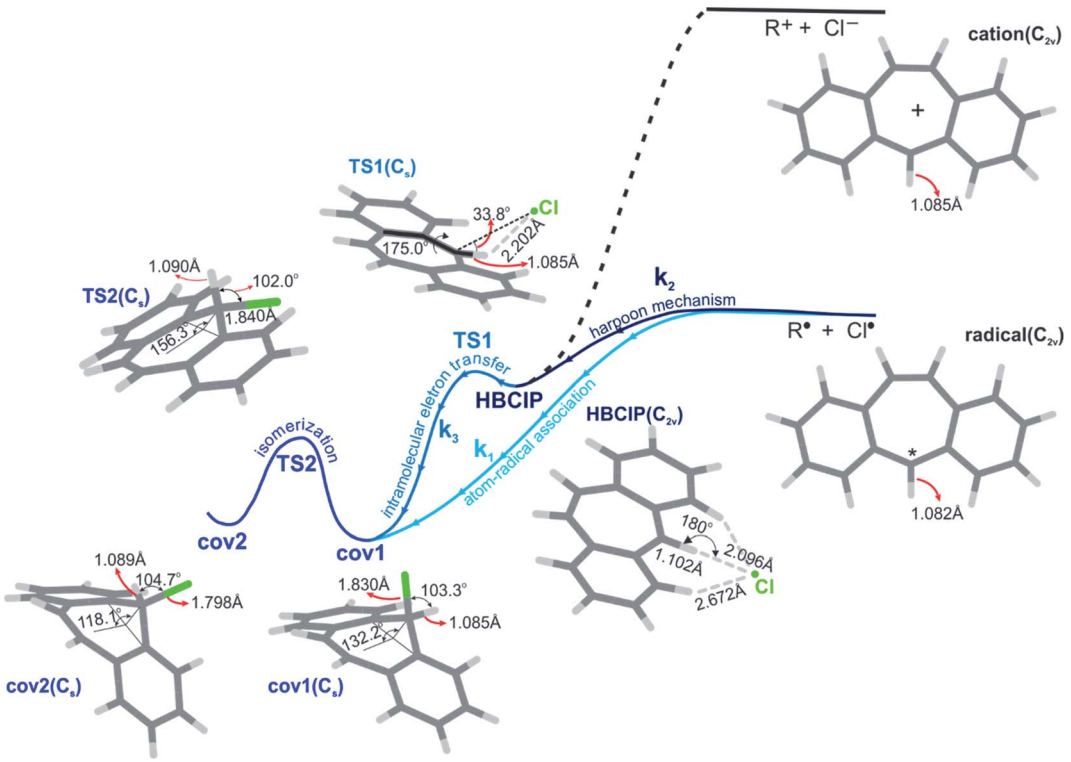

Fig. 1 Qualitative relative gas-phase energies and reaction profiles for the systems studied in this work. See Table 1 for the computed free energies. The elementary steps are also given. All given bond distances and angles have been obtained at the M05-2X/6-311++G** level (without BSSE). The C atom indicated by * is the one containing the unpaired electron. The Cartesian coordinates of all structures are given in the ESI.†

for the 6-31++G** and 6-31++G**(H,Cl)/6-31++G**(C) basis set, respectively (see Table 1).

Although significant variations have been observed for the free energy barriers of the cov1 → HBCIP and cov1 → cov2 reactions (given by the TS1 and TS2 values in Table 1, respectively), the corresponding barrier for the HBCIP → cov1 reaction is in a much sharper range, from 1.03 to 1.62 kcal mol^{-1} (see Table 1).

The computed CPCM free energy difference between cov1 and the HBCIP in toluene (at −80 °C) is 20.72 kcal mol^{-1}. This value can be used to estimate the equilibrium constant (and thus the [HBCIP]/[cov1] ratio) for the cov1 → HBCIP reaction, yielding [HBCIP]/[cov1] ∼ 10^{-37}, which means that [HBCIP] is negligible, as compared to [cov1]. Although this ratio can change significantly with the solvation method, it is expected that it is maintained very small, and thus [HBCIP] remains negligible. Preliminary calculations for k_3 yields a value of ∼10^{11} s^{-1}. The results obtained for k_3 and [HBCIP]/[cov1] can explain the absence of any NMR-signal due to the dibenzo[*a*,*d*]tropylium cation in the NMR spectrum of 5-chloro-5*H*-dibenzo[*a*,*d*]cycloheptene in toluene at −80 °C.[60] As the authors suggested, the k_3 rate constant is very fast on the NMR time scale. Even if

Table 1 Gas-phase Δ*G* values (at 0.4 K, in kcal mol^{-1}) of the studied structures, obtained at the DFT and MP2 levels

Δ*G*						
Level		M05-2X			MP2	
Basis set		6-31++G**	6-31++G**(H,Cl)/6-31++G**(C)	6-311++G**	6-31++G**	6-31++G**(H,Cl)/6-31++G**(C)
Structure or channel	cov1[a]	0.00	0.00	0.00	0.00	0.00
	cov2[a]	0.67	0.87	0.79	1.28	1.55
	HBCIP[a]	30.96 (31.13)[b]	31.00 (31.48)[b]	32.62 (33.13)[b]	38.16 (43.84)[b]	39.38 (45.69)[b]
	TS1[a]	32.19 (32.42)[b]	32.12 (32.70)[b]	33.65 (34.19)[b]	39.57 (45.46)[b]	40.45 (47.18)[b]
	TS2[a]	15.71	15.78	16.18	19.17	19.17
	R$^{\bullet}$ +·Cl$^{\bullet}$	65.06	—[c]	66.25	71.47	—[c]
	R^{+} +·Cl^{-}	116.56	—[c]	118.77	127.36	—[c]

[a] See Fig. 1 for the structures associated with these labels. [b] Values in parenthesis have been computed including BSSE. [c] Values not computed due to the different basis sets used for the separated fragments.

this were not the case, the tiny relative value of [HBCIP] would preclude its detection by this technique. Our group just started a study to compute the rate constants k_1, k_2, and k_3 (of the suggested mechanism, as discussed later) along with a kinetic modeling which includes the time dependence of [HBCIP].

Taking the C–Cl bond dissociation energy (BDE) of benzyl chloride as a reference value to test the accuracy of some of the calculations performed in this work, one obtains a BDE value between 97 and 100 kcal mol^{-1} (with the same methods and basis sets given in Table 1) in good agreement with the experimental value of 95 kcal mol^{-1}.[79] Thus, it is expected that the values between ~65 (DFT) and 71 (MP2) kcal mol^{-1} can be considered good estimates of the C–Cl BDE of cov1 (see Table 1). The computed ΔG values for the R–Cl → R$^{\bullet}$ + ·Cl$^{\bullet}$ reaction should be very close to BDE, as the thermal corrections are almost null due to the very low temperature (0.4 K).

The experimental adiabatic ionization energy (AIE) of the cycloheptatrien-1-yl radical (or tropyl) is 6.28 eV.[80] The computed values (using the same methods and basis sets given in Table 1) vary from 5.77 to 6.17 eV. The best agreement has been obtained at the M05-2X level, with values of 6.09 and 6.17 eV for the 6-31++G** and 6-311++G** basis sets, respectively. At the MP2 level, the corresponding values are 5.77 and 5.93 eV. As in the case of the dibenzo[*a*,*d*]tropyl radical, the results for the tropyl at the MP2 level have been obtained using the geometries optimized at the M05-2X level. As explained before, in the case of the radical, this choice is due to the absence of analytical gradient at the ROMP2 level and the high spin contamination at the UMP2 level, and for the cation, the M05-2X geometry has been chosen for the sake of consistency. A possible explanation for larger differences found for the MP2 AIE results is that accurate calculations at this level generally require larger (*e.g.*, correlation consistent with a sufficient number of diffuse functions) basis sets. Thus, if the MP2 calculation is now performed with the aug-cc-pVTZ basis set, one obtains 6.10 eV, in much better agreement with the experimental value than those obtained with the 6-31++G** (5.77 eV) and 6-311++G** (5.93 eV) basis sets. However, the use of the aug-cc-pVTZ basis set for the structures studied in this work is computationally prohibitive at the MP2 level. Besides, for preliminary calculations performed with both aug-cc-pVDZ and aug-cc-pVTZ basis sets for the HBCIP, all attempts to reach convergence at the SCF level failed. Thus, the 6-31++G** and 6-311++G** basis sets have been chosen instead.

Another important property is the electron affinity (EA) of Cl$^{\bullet}$, whose experimental value is 3.62 eV.[81] The computed values with the 6-31++G**/6-311++G** basis sets are 3.74/3.77 and 3.17/3.18 eV at the M05-2X and MP2 levels, respectively. Therefore, the accuracy of the M05-2X results is similar for both AIE of tropyl radical and EA of Cl$^{\bullet}$. The same holds at the MP2 level.

Based on the previously mentioned set of reference results (for the BDE of C_6H_5–Cl, AIE of tropyl radical, and EA of Cl$^{\bullet}$), it is expected that the obtained results (especially at the M05-2X level) are accurate enough to correctly describe the energetic of the studied structures and the dissociation channels.

The computed values for the AIE of the dibenzo[*a*,*d*]tropyl radical (R$^{\bullet}$) with the 6-31++G**/6-311++G** basis sets are 5.98/6.04 and 5.59/5.74 eV at the M05-2X and MP2 levels, respectively. The AIE values of R$^{\bullet}$ are slightly smaller than those of the tropyl radical, by 0.11 to 0.19 eV. The ionization energy of the tropyl radical is one of the lowest ever reported for a hydrocarbon radical[82] due to the very high stability of the tropylium cation. Surprisingly, the inclusion of two ring-fused phenyl rings to the tropyl radical leads to a small (though not negligible) decrease of the AIE.

The differences between the M05-2X and MP2 results for the AIE(R$^{\bullet}$) are close to those obtained for the tropyl radical. The calculated difference between ionic ($R^+ + Cl^-$) and neutral (R$^{\bullet}$ + Cl$^{\bullet}$) dissociation channels is given by the difference between the AIE(R$^{\bullet}$) and EA(Cl$^{\bullet}$). Although results at the MP2/6-311++G** level are absent from Table 1, one can use the AIE(R$^{\bullet}$) and EA(Cl$^{\bullet}$) results at this level to compute the energy difference between the ionic and neutral dissociation channels, yielding 2.57 eV (59.03 kcal mol^{-1}). The corresponding results at the MP2/6-31++G**, M05-2X/6-31++G** and M05-2X/6-311++G** levels are 2.42 eV (55.89 kcal mol^{-1}), 2.23 eV (51.50 kcal mol^{-1}), and 2.28 eV (52.52 kcal mol^{-1}), respectively (see Table 1).

Characterization of the HBCIP

The structure of the HBCIP studied in this work is shown in Fig. 1. Tests with tropylium and benzotropylium cations forming HBCIP with Cl$^-$ (in planar structures similar to that of HBCIP in Fig. 1) did not lead to a minimum. The number of hydrogen bonds is one and two for the tropylium/Cl$^-$ and benzotropylium/Cl$^-$ ion pairs, respectively. As in the case of the HBCIP shown in Fig. 1, one has three hydrogen bonds; it seems that this is the minimum number of H bonds required for a stable (or, more appropriately, metastable) and planar HBCIP formed between an aromatic hydrocarbon carbocation and a chloride anion. However, confirmation of such a hypothesis requires further studies. An additional analysis of the three H bonds of the HBCIP is included in the ESI.†

The dipole moment of the HBCIP varies from ~14.2 to 14.5 D, depending on the method and basis set. Conversely, in the case of the covalent structures, the corresponding values are much smaller, varying from ~1.9 to 2.3 D. Thus, the HBCIP is a highly polar structure, as for $[CH_3]^+Cl^-$ (ref. 47) and $[C_2H_5]^+Cl^-$,[50] the two examples of HBCIP containing hydrocarbon carbocations studied by our group. The HBCIP studied in this work should be more accurately represented by $R^{\delta+}Cl^{\delta-}$. The computed NBO charges vary from ~0.86 to 0.88, depending on the computational level. On the other hand, for the covalent structures the corresponding δ values vary from ~0.01 to 0.07, indicating a much larger charge separation for the HBCIP, which is consistent with its much larger dipole moment.

The binding energy (BE) of HBCIP is given by the difference between the energies of the ionic channel and that of HBCIP, as shown in eqn (1). As can be seen from Table 1, the values at the M05-2X level (without BSSE) are 85.6 and 86.15 kcal mol^{-1}, with the 6-31++G** and 6-311++G** basis sets, respectively. With BSSE, these values change slightly, to 85.43 and 85.64 kcal mol^{-1}. On the other hand, at the MP2 level, the effect of BSSE is much larger, changing the binding energy from 89.2

to 83.52 kcal mol^{-1}, with the 6-31++G** basis set. The set of values obtained here are intermediate between those of the ion pairs found for chloromethane (99.16 kcal mol^{-1} (ref. 47)) and chloroethane (75.64 kcal mol^{-1} (ref. 50)), but with a significant qualitative difference: *the HBCIP between dibenzo[a,d]tropylium cation and Cl$^-$ can be formed in the ground state*.

$$\mathrm{BE(HBCIP)} = E(\mathrm{R^+}) + E(\mathrm{Cl^-}) - E(\mathrm{HBCIP}) \quad (1)$$

As pointed out by Hunt *et al.*,[44] in doubly ionic H bonded systems, one should not relate the total association (or binding) energy with the H-bond strength. For the HBCIP studied in this work, such correlation would erroneously lead to the conclusion that very strong H bonds are present, which is not the case. However, if the very large attractive coulombic interaction of ~76.8 kcal mol^{-1} (obtained using a distance of 4.355 Å between the ions, as explained below) is discounted from the M05-2X/6-311++G**values of 85.64 and 86.15 kcal mol^{-1} (obtained with and without BSSE, respectively), total H-bond energies of ~8.8 and 9.3 kcal mol^{-1} are obtained. As there are three H bonds, an average value of ~3 kcal mol^{-1} per H bond is obtained. This value is very close to that obtained for the HBCIP of chloroethane, a system with a weak H bond.[50] Besides, from the values shown in Fig. 1, one gets an average H bond distance of 2.480 Å, only 0.032 Å smaller than that obtained for the HBCIP of chloroethane.[50]

Due to the near degeneracy of the Cl lone pairs, the three lowest excited singlet states (*i.e.*, charge recombination (CR) states) of the HBCIP are almost degenerate, and their excitation energies and oscillator strengths (computed at the TD-CAM-B3LYP level) are given in Table 2. $2p_\sigma$(C) is the empty 2p orbital which was singly occupied in the radical. $2p_\sigma$(C) is the LUMO orbital, and σ stands for the sigma bond formed by this orbital in the covalent structures. The calculations have been performed at each one of the obtained geometries, with the same basis sets used for the geometry optimizations. The frontier molecular orbitals mentioned in Table 2 are depicted in Fig. 2.

As can be seen from Table 2, the three excited states are in the near-infrared, and among them, CR2 (dominated by the HOMO → LUMO transition) is the one that is more suitable to be used to identify the HBCIP due to its largest *f* value. The obtained results are slightly dependent on the geometry and basis set, especially at the M05-2X level. Even at the MP2 level, the effect is small, with the main variation obtained when one compares the results using the geometries optimized with and without BSSE. In this case, the ΔE_{CR} values change by at most 0.12 eV. It is worth mentioning that the CR band expected for the HBCIP studied in this work is associated with a process which is the reverse of what is commonly observed, that is, instead of charge separation, one has charge recombination, $\mathrm{R^+Cl^-} \xrightarrow{h\nu} \mathrm{R{\bullet}Cl{\bullet}}$.

The energy of the CR transition can be estimated through a modification of eq. (3.25) from ref. 83. As one has charge recombination, the signs of the three terms on the right side of that equation must change, yielding:

$$\Delta E_{CR} = \mathrm{EA(Cl{\bullet})} - \mathrm{VIE(R{\bullet})} + \frac{e^2}{R_{DA}}, \quad (2)$$

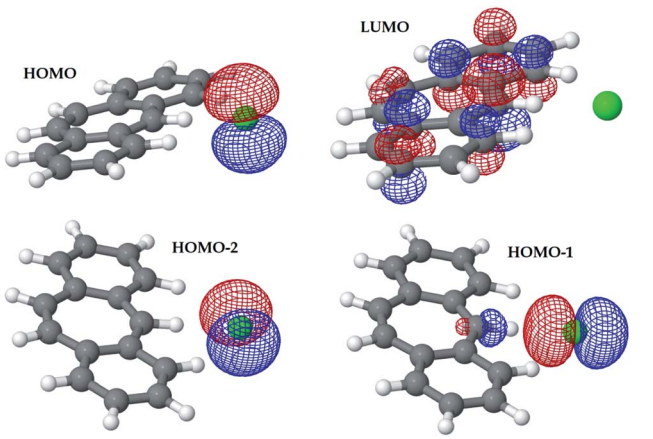

Fig. 2 Frontier molecular orbitals mentioned in Table 2, computed at the M05-2X/6-31++G** level.

Table 2 Computed excitation energies (ΔE_{CR}, in eV) and oscillator strengths (*f*) for the CR states of HBCIP, at the TD-CAM-B3LYP level. Unless stated otherwise, M05-2X geometries have been used

Basis sets									
	6-31++G**			6-311++G**(H,Cl)/6-31++G**(C)			6-311++G**		
States	CR1	CR2	CR3	CR1	CR2	CR3	CR1	CR2	CR3
f	$<10^{-4}$ $(<10^{-4})^a$ $(1.0 \times 10^{-4})^b$ $(<10^{-4})^{a,b}$	6.2×10^{-3} $(6.2 \times 10^{-3})^a$ $(5.9 \times 10^{-3})^b$ $(5.4 \times 10^{-3})^{a,b}$	$<10^{-4}$ $(<10^{-4})^a$ $(<10^{-4})^b$ $(<10^{-4})^{a,b}$	$<10^{-4}$ $(<10^{-4})^a$ $(2 \times 10^{-4})^b$ $(1.0 \times 10^{-4})^{a,b}$	6.2×10^{-3} $(6.1 \times 10^{-3})^a$ $(6.1 \times 10^{-3})^b$ $(5.5 \times 10^{-3})^{a,b}$	$<10^{-4}$ $(<10^{-4})^a$ $(<10^{-4})^b$ $(<10^{-4})^{a,b}$	$<10^{-4}$ $(<10^{-4})^a$	6.3×10^{-3} $(6.3 \times 10^{-3})^a$	$<10^{-4}$ $(<10^{-4})^a$
ΔE_{CR}	1.35 (1.34)^a (1.40)^b (1.33)^{a,b}	1.50 (1.50)^a (1.56)^b (1.44)^{a,b}	1.54 (1.54)^a (1.60)^b (1.49)^{a,b}	1.35 (1.34)^a (1.43)^b (1.35)^{a,b}	1.50 (1.49)^a (1.61)^b (1.48)^{a,b}	1.54 (1.53)^a (1.64)^b (1.52)^{a,b}	1.32 (1.31)^a	1.45 (1.46)^a	1.50 (1.50)^a
DC^c	HOMO−1 → LUMO	HOMO → LUMO	HOMO−2 → LUMO	HOMO−1 → LUMO	HOMO → LUMO	HOMO−2 → LUMO	HOMO−1 → LUMO	HOMO → LUMO	HOMO−2 → LUMO

^{a} Values computed using the BSSE geometries. ^{b} Values computed using the MP2 geometries. ^{c} Dominating configuration.

where VIE(R$^{\bullet}$) is the vertical ionization energy of the dibenzo[*a*,*d*]tropyl radical (R$^{\bullet}$), and the last term refers to the coulombic attraction energy lost due to the charge recombination. Due to the resonance of the double bonds, the charge center is delocalized over all C atoms. Thus, it is assumed that the charge center of the cation is on its center of mass. Consequently, R_{DA} is defined as the distance between the center of mass of R$^{\bullet}$ and Cl$^{\bullet}$. As shown in Fig. 3, the energy of the lowest-lying CR state is slightly lower than that of the neutral channel. From the point of view of the HBCIP, the CR states can be described as those resulting from a "head-on" approximation between R$^{\bullet}$ and Cl$^{\bullet}$, along the C_2 symmetry axis but without any charge transfer.

From the previous discussion concerning the AIE of tropyl radical, it is expected that the M05-2X results should be more reliable than the MP2 results also for the dibenzo[*a*,*d*]tropyl radical. Thus, using the M05-2X/6-31++G** values of 6.00 eV, 3.74 eV, and 4.353 Å for VIE(R$^{\bullet}$), EA(Cl$^{\bullet}$), and R_{DA}, respectively, one obtains $\Delta E_{CR} = 1.07$ eV, in relatively good agreement with the lowest ΔE_{CR} value (of 1.35 eV, see Table 2). The corresponding M05-2X results obtained with the 6-311++G** basis set are 6.07 eV, 3.77 eV, and 4.355 Å, yielding the same previous ΔE_{CR} value (1.07 eV), which is again in relatively good agreement with the computed value (of 1.32 eV). The corresponding computed R_{DA} values, including BSSE, are 4.355 Å, with both basis sets. The agreement between the TD-DFT results and those computed with eqn (2) gives us some confidence in using this equation to estimate ΔE_{CR} for HBCIP formed between much larger aromatic hydrocarbon carbocations and chloride, with a considerably lower computational cost (as the TD-DFT calculation may not be needed).

Another essential property of the HBCIP studied in this work is its characteristic vibrational modes. It is expected that at least two of them maybe used to identify this species. One is in the far-infrared region (in ~160 cm^{-1}), an intermolecular cation–anion mode of intermediate intensity also observed for the corresponding ion pairs of CF_3–CH_2Cl[49] and chloroethane.[50] The other is the red shifted C–H mode in the **C^{+}–H**···Cl^{-} complex due to H bond formation, with an expected much-increased intensity compared to the corresponding C–H stretching mode observed for the covalent structures. Upon formation of the HBCIP, this frequency decreases from ~3100 to 2900 cm^{-1}. This red shift for the C–H stretching mode is consistent with C–H bond elongation[84] (and its weakening due to the H···X interaction). Furthermore, the uncommonly large red shift for a **C–H**···X motif (where X is an electronegative element) is probably due to the occurrence of a doubly ionic hydrogen bond.[44] The computed vibrational frequencies (at the M05-2X/6-311^{++}G** level) of cov1, cov2, and HBCIP are given in the ESI.†

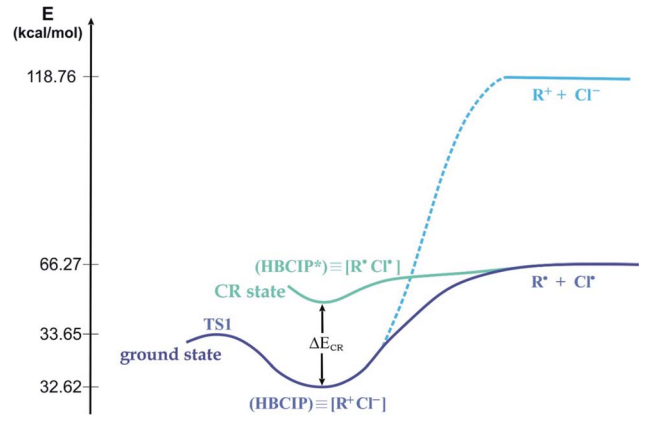

Fig. 3 Scheme showing the lowest lying CR state, at the HBCIP geometry. The correlation between this state and the neutral dissociation channel is also shown. The energy values given have been computed at the M05-2X/6-311++G** level (see Table 1).

Suggested mechanism

The elementary step for the HBCIP formation, which is assumed to be described by the harpoon mechanism, is considered as a competing reaction for the formation of the covalent (R–Cl) structure, cov1 (see Fig. 1). Accordingly, the proposed mechanism (for the reaction between R$^{\bullet}$ and Cl$^{\bullet}$ within the He nanodroplets) has the following steps:

$$R^{\bullet} + Cl^{\bullet} \rightarrow \text{cov1}, k_1 \text{ (atom radical association).} \quad (3)$$

$$R^{\bullet} + Cl^{\bullet} \rightarrow R^{+}Cl^{-}, k_2 \text{ (harpoon mechanism).} \quad (4)$$

$$R^{+}Cl^{-} \rightarrow \text{cov1}, k_3 \text{ (intramolecular electron transfer).} \quad (5)$$

$$\text{cov1} \rightarrow \text{cov2 (isomerization).} \quad (6)$$

$$\text{cov2} \rightarrow \text{cov1 (isomerization).} \quad (7)$$

If both conditions are satisfied: (i) very low temperatures (low kinetic energies) and (ii) very efficient vibrational relaxation of the R$^{\bullet}$ radical within the He nanodroplets, one can disregard other reactions as, for instance, H atom abstraction, due do its presumably high dissociation energy. Besides, due to the very large barriers, the reverse of reactions (4) and (5) can also be disregarded. As shown in Table 2, these two free energy barriers are ~33 kcal mol^{-1}. Other reactions that can be neglected comprise the radical–radical (R$^{\bullet}$ + R$^{\bullet}$) and atom–atom (Cl$^{\bullet}$ + Cl$^{\bullet}$) recombination, which can be achieved through trapping one single R$^{\bullet}$ and Cl$^{\bullet}$ species within He nanodroplets, as explained later.

In the first elementary step (which is an atom-radical association reaction), it is expected that cov1 (see Fig. 1) were the covalent structure formed preferentially from the neutral fragments. Such an assumption is based on the pseudo-axial position of the C–Cl bond in cov1, which is consistent with the perpendicular orientation of the C p(π) orbital containing the unpaired electron of the radical (see Fig. 1). This C atom is indicated as C* in Fig. 1. Another possible reason for the assumed preferential formation of cov1 is the lower deviation from planarity of the central ring of cov1, as compared to that of cov2. For cov1 and cov2, one has deviations from planarity of 47.8 (=180 − 132.2) and 61.9 (=180 − 118.1) degrees, respectively (see Fig. 1). After cov1 is formed, part of the molecules can rearrange to the less stable cov2 (see Fig. 1) and, when in equilibrium, the [cov1]/[cov2] ratio is determined by the free energy difference between cov1 and cov2.

The second step can be considered an example of the harpoon mechanism.[85] Although a charge-transfer reaction can take place at relatively large distances (as discussed below) and at several orientations between R$^{\bullet}$ and Cl$^{\bullet}$, the formation of the HBCIP requires not only a planar encounter between the fragments but also a "head-on" approach along the C_2 symmetry axis (see Fig. 1). The importance of the orientational effect for the harpoon mechanism has been recognized in several systems.[86–92] Clearly, the occurrence of H bonds is very important for the stability of HBCIP. These bonds can be interpreted as a "lock" that holds the opposite charged ions relatively close to each other (as can be seen in Fig. 1, for HBCIP, the distance between the C atom which is in the C_2 axis and the Cl atom is ~3.20 Å, at the M05-2X/6-311++G** level). Out-of-plane vibrational modes can open this "lock" and leads to the covalent structure (cov1).

One can estimate the maximum distance (d^*, in Å, between the charge centers) consistent with a favorable CT reaction between R$^{\bullet}$ and Cl$^{\bullet}$ [ref. 85, p. 416] from

$$d^* = \frac{1.44}{[\mathrm{VIE}(R\bullet) - \mathrm{EA}(\mathrm{Cl}\bullet)]}, \quad (8)$$

This equation includes the attractive coulombic energy of the formed ion pair, and VIE(R$^{\bullet}$) and EA(Cl) are in eV. The computed values of VIE(R$^{\bullet}$) and EA(Cl$^{\bullet}$) at the M05-2X/6-311++G** level are 6.07 and 3.77 eV, respectively, which yields $d^* = 6.261$ Å. d^* is a very important quantity for rate constant calculations associated with the harpoon mechanism.[85] This relatively large distance between the charge centers (the C* and Cl atoms, see Fig. 1) indicates that the charge-transfer between the neutral fragments can take place long before the H bonds are formed, as in the HBCIP the distance between these two atoms is ~3.20 Å (at the M05-2X/6-311++G** level, see Fig. 1).

Probing the HBCIP in He nanodroplets

Helium nanodroplets (HND) seem to be a suitable environment for probing the HBCIP studied in this work. The experimental setup allows excellent control of reactant incorporation into each droplet at a molecular level.[93–95] The rapid cooling inside the HND, along with the very low temperature and the sequential pickup technique, allow kinetic trapping of entrance and exit 1:1 complexes corresponding to very shallow local minima.[93,95] Thus, non-equilibrium distributions can be achieved. The experimental conditions have been optimized for the pickup of single radicals in molecule–radical reactions[96–98] or single Cl atom in the Cl + HCN[99] and Cl + HCl reactions.[100] One of the lowest energy barriers able to kinetically trap metastable species lies near 100 cm^{-1} (~0.3 kcal mol^{-1}).[101] Infrared spectroscopy has been used to probe structures of the formed metastable species,[93–96,99,101–105] in several cases including the Stark effect to determine the permanent dipole moments of the systems within the HNDs.[93,95,99,101,102,105] In several examples, the entrance channel is more stable than the separated reactants, and the corresponding complex is formed barrierlessly.[99,102–106]

Our suggestion is to use this technique to induce formation of HBCIP as well as to trap it and to probe its formation. If the ion pair can survive for enough time (~1 ms) before the equilibrium distribution is achieved, in principle it could be detected by infrared spectroscopy[95] due to its characteristic intense C^+–H···Cl^- intermolecular vibration in the far-infrared region (~160 cm^{-1}), as the HND technique has already been adapted for far-infrared spectroscopy.[107] Besides, the very high dipole moment (~14 D) of the HBCIP can be measured using the Stark effect, as mentioned before. Its most intense CR band in the near-infrared region (~1.50 eV) can also be used for its detection.[93,94]

Although atom-radical reactions are absent from the previous studies, they include radical[96–98] and Cl atom generation.[99,100] Thus, it is expected that the experience gained with radical and Cl atom generation as well as with sequential pickup of such species within HND can be adapted to study the single-molecule reaction between the 1,2:4,5-dibenzotropyl radical and the Cl atom. It would allow identifying the HBCIP because after pickup of this radical one expects a rapid quenching of its internal[95,102,105,108] and translational[108] degrees of freedom (due to evaporation of He atoms[109]). Cooling of the translational degrees of freedom of Cl after its pickup is also expected.[108] Consequently, the reactive encounter between 1,2:4,5-dibenzotropyl radical and the Cl atom takes place as both fragments have minimal energies, thus preventing side reactions as H atom abstraction by the Cl atom. It is estimated a release of ~33 kcal mol^{-1} (at the M05-2X/6-311++G** level, see Table 1) upon the formation of the HBCIP from the 1,2:4,5-dibenzotropyl radical and the Cl atom. This value is consistent with the evaporation of ~2357 He atoms.[109] If this evaporation rate is higher than that of interconversion from the HBCIP to the covalent form, then the former species can be trapped and thus detected.[99,101]

Formation of the covalent compound from the neutral fragments is much more exothermic than the formation of the HBCIP, leading to a release of ~66 kcal mol^{-1} (for cov1 at the M05-2X/6-311++G** level, see Table 1), a value which is still not high enough to eject the molecule from the HND,[98] and it is consistent with evaporation of ~4714 He atoms.[109] Therefore, in principle, it is possible to distinguish between the R$^{\bullet}$ + Cl$^{\bullet}$ → R–Cl and R$^{\bullet}$ + Cl$^{\bullet}$ → R^+Cl^- elementary reactions from a mass measurement after a reactive encounter between the fragments.[110]

Conclusions

Formation of a ground-state hydrogen-bonded contact ion pair (HBCIP) in the gas phase *via* the harpoon mechanism, through a reaction between the 1,2:4,5-dibenzotropyl radical (R$^{\bullet}$) and Cl$^{\bullet}$ is suggested (supported by DFT and MP2 calculations). It is the first modeling study to find computational evidence for the possibility of a gas-phase 'hydrocarbon carbocation'-containing HBCIP (R^+Cl^-) in the ground state.

Formation of R^+Cl^- from the neutral fragments (R$^{\bullet}$ and Cl$^{\bullet}$) releases ~33 kcal mol^{-1} of energy. It is accompanied by the formation of three H bonds with chloride (see Fig. 1), and its binding energy of ~86 kcal mol^{-1} is mainly coulombic. Each H bond contributes with ~3 kcal mol^{-1} per H bond (results

obtained at the M05-2X/6-311++G** level), a value characteristic of weak H bonds. Though weak, these bonds can be interpreted as a "lock", which holds the opposite charged ions relatively close (see Fig. 1).

The formation of R^+Cl^- is expected to compete with the formation of a covalent structure, R–Cl. R^+Cl^- is ~33 kcal mol^{-1} less stable than R–Cl, with a very small $R^+Cl^- \rightarrow$ R–Cl interconversion barrier of ~1 kcal mol^{-1} (values obtained at the M05-2X/6-311++G** level).

R^+Cl^- is a highly polar system with a dipole moment of ~14 D, has C_{2v} symmetry (see Fig. 1), and two characteristic vibrational modes. One is in the far-infrared region (in ~160 cm^{-1}), an intermolecular cation–anion mode of intermediate intensity, while the other is the red shifted C–H mode in the $\mathbf{C^+–H\cdots Cl^-}$ complex due to H bond formation, with an expected much-increased intensity compared to the corresponding C–H stretching mode observed for the covalent structures.

Upon the formation of the HBCIP, this frequency decreases from ~3100 to 2900 cm^{-1}. The uncommonly large red shift for a **C–H**···X motif (where X is an electronegative element) can be explained by the presence of a doubly ionic hydrogen bond.[44]

The HBCIP has three very close charge recombination transitions in the near-infrared region (at ~1.3 to 1.5 eV). The most intense transition (at ~1.4–1.5 eV) has an oscillator strength of 6.3×10^{-3} (values obtained at the CAM-B3LYP/6-311++G** level).

Identification of such a new kind of ion-pair using the above mentioned properties through a highly controlled reaction (at a molecular level) between $R^\bullet$ and $Cl^\bullet$ inside He nanodroplets is very likely and it is also discussed. This likeliness is due to the fact that this technique allows achievement of non-equilibrium distributions and it has already been coupled to setups suited for the described properties.

Conflicts of interest

There are no conflicts to declare.

Acknowledgements

E. V. thanks the Brazilian agency CNPq (Grant Number 303884/2018-5 and 423112/2018-0) for support. The remaining authors thank to the Brazilian agencies CAPES and FINEP for financial support. They are also thankful to M. Barbatti for the very useful discussion and to the CENAPAD-SP/Unicamp and LRC/Cenapesq supercomputing centers for the computational facilities.

References

1 A. Maccoll and P. J. Thomas, *Nature*, 1955d, **176**, 392–393.
2 C. F. Ingold, *Proc. Chem. Soc.*, 1957, 279–287.
3 A. Maccoll, *Theoretical Organic Chemistry*, Butterworths, London, 1958, p. 230.
4 A. Maccoll, in *The Transition State*, special publication no. 16, The Chemical Society, London, 1962.
5 C. K. Ingold, *Structure and Mechanism in Organic Chemistry*, G. Bell and Sons, Ltd., London, 1963.
6 A. Maccoll, *Adv. Phys. Org. Chem.*, 1965, **3**, 91–122.
7 A. Maccoll and P. J. Thomas, *Prog. React. Kinet.*, 1967, **4**, 119.
8 A. Maccoll, *Chem. Rev.*, 1969, **69**(1), 33–60.
9 T. H. Morton, *Tetrahedron*, 1982, **38**, 3195–3243.
10 G. Chuchaniand and R. M. Dominguez, *Int. J. Chem. Kinet.*, 1983, **15**, 795–803.
11 G. Chuchani, A. Rotinov, R. M. Dominguez and N. González, *J. Org. Chem.*, 1984, **49**, 4157–4160.
12 G. Chuchani, R. M. Dominguez and A. Rotinov, *Int. J. Chem. Kinet.*, 1986, **18**, 203–213.
13 G. Chuchani, R. M. Dominguez and I. Martín, *React. Kinet. Catal. Lett.*, 1986, **30**, 77–83.
14 G. Chuchani and I. Martin, *J. Phys. Chem.*, 1986, **90**, 431–433.
15 G. Chuchani and R. M. Dominguez, *J. Phys. Chem.*, 1987, **91**, 1883–1887.
16 G. Chuchani and A. Rotinov, *Int. J. Chem. Kinet.*, 1989, **21**, 367–371.
17 A. A. Turnipseed and J. W. Birks, *J. Phys. Chem.*, 1991, **95**, 6569–6574.
18 G. Chuchaniand and R. M. Dominguez, *J. Chem. Soc., Perkin Trans. 2*, 1993, 1295–1298.
19 G. Chuchani, A. Rotinov, R. M. Dominguez and I. Martin, *J. Phys. Org. Chem.*, 1996, **9**, 348–354.
20 Y. Brusco, N. Berroteran, M. Loroño, T. Córdova and G. Chuchani, *J. Phys. Org. Chem.*, 2009, **22**, 1022–1029.
21 E. Marquez, J. R. Mora, T. Cordova and G. Chuchani, *Int. J. Chem. Kinet.*, 2011, **43**, 537–546.
22 M. M. Tosta, J. R. Mora, T. Cordova and G. Chuchani, *J. Comput. Methods Sci. Eng.*, 2012, **12**, 237–245.
23 O. Brea, M. Loroño, E. Marquez, J. R. Mora, T. Cordova and G. Chuchani, *Int. J. Quantum Chem.*, 2012, **112**, 2504–2514.
24 M. Luiggi, J. R. Mora, M. Loroño, E. Marquez, J. Lezama, T. Cordova and G. Chuchani, *Comput. Theor. Chem.*, 2014, **1027**, 165–172.
25 R. J. Guerra, J. Lezama, T. Cordova-Sintjago and G. Chuchani, *Mol. Phys.*, 2018, **116**(9), 1118–1126.
26 J. P. Leal, J. M. S. S. Esperança, M. E. Minas da Piedade, J. N. C. Lopes, L. P. N. Rebelo and K. R. Seddon, *J. Phys. Chem. A*, 2007, **111**, 6176–6182.
27 R. W. Berg, A. Riisager and R. Fehrmann, *J. Phys. Chem. A*, 2008, **112**, 8585–8592.
28 J. H. Gross, *J. Am. Soc. Mass Spectrom.*, 2008, **19**, 1347–1352.
29 N. Akai, D. Parazs, A. Kawai and K. Shibuya, *J. Phys. Chem. B*, 2009, **113**, 4756–4762.
30 N. Akai, A. Kawai and K. Shibuya, *J. Phys. Chem. A*, 2010, **114**, 12662–12666.
31 K. R. J. Lovelock, A. Deyko, P. Licence and R. G. Jones, *Phys. Chem. Chem. Phys.*, 2010, **12**, 8893–8901.
32 A. W. Taylor, K. R. J. Lovelock, A. Deyko, P. Licence and R. G. Jones, *Phys. Chem. Chem. Phys.*, 2010, **12**, 1772–1783.
33 C. Wang, H. Luo, H. Li and S. Dai, *Phys. Chem. Chem. Phys.*, 2010, **12**, 7246–7250.
34 A. Deyko, K. R. J. Lovelock, P. Licence and R. G. Jones, *Phys. Chem. Chem. Phys.*, 2011, **13**, 16841–16850.
35 F. Malberg, A. S. Pensado and B. Kirchner, *Phys. Chem. Chem. Phys.*, 2012, **14**, 12079–12082.

36 F. Malberg, M. Brehm, O. Hollóczki, A. S. Pensado and B. Kirchner, *Phys. Chem. Chem. Phys.*, 2013, **15**, 18424–18436.
37 E. I. Obi, C. M. Leavitt, P. L. Raston, C. P. Moradi, S. D. Flynn, G. L. Vaghjiani, J. A. Boatz, S. D. Chambreau and G. E. Douberly, *J. Phys. Chem. A*, 2013, **117**, 9047–9056.
38 T. Ogura, N. Akai, A. Kawai and K. Shibuya, *Chem. Phys. Lett.*, 2013, **555**, 110–114.
39 K. Dong, L. Zhao, Q. Wang, Y. Song and S. Zhang, *Phys. Chem. Chem. Phys.*, 2013, **15**, 6034–6040.
40 B. Brunetti, A. Ciccioli, G. Gigli, A. Lapi, N. Misceo, L. Tanzid and S. V. Ciprioti, *Phys. Chem. Chem. Phys.*, 2014, **16**, 15653–15661.
41 K. R. J. Lovelock, J. P. Armstrong, P. Licence and R. G. Jones, *Phys. Chem. Chem. Phys.*, 2014, **16**, 1339–1353.
42 L. H. Finger, F. Wohde, E. I. Grigoryev, A.-K. Hansmann, R. Berger, B. Roling and J. Sundermeyer, *Chem. Commun.*, 2015, **51**, 16169–16172.
43 K. Hanke, M. Kaufmann, G. Schwaab, M. Havenith, C. T. Wolke, O. Gorlova, M. A. Johnson, B. P. Kar, W. Sanderc and E. Sanchez-Garcia, *Phys. Chem. Chem. Phys.*, 2015, **17**, 8518–8529.
44 P. A. Hunt, C. R. Ashworth and R. P. Matthews, *Chem. Soc. Rev.*, 2015, **44**, 1257–12889.
45 A. M. Dunaev, V. B. Motalov, L. S. Kudin and M. F. Butman, *J. Mol. Liq.*, 2016, **219**, 599–601.
46 K. Low, S. Y. S. Tan and E. I. Izgorodina, *Front. Chem.*, 2019, **7**, 208.
47 V. C. de Medeiros, R. B. de Andrade, E. F. V. Leitão, E. Ventura, G. F. Bauerfeldt, M. Barbatti and S. A. do Monte, *J. Am. Chem. Soc.*, 2016, **138**, 272–280.
48 V. C. de Medeiros, R. B. de Andrade, G. P. Rodrigues, G. F. Bauerfeldt, E. Ventura, M. Barbatti and S. A. do Monte, *J. Chem. Theory Comput.*, 2018, **14**, 4844–4855.
49 G. P. Rodrigues, T. M. L. de Lima, R. B. de Andrade, E. Ventura, M. Barbatti and S. A. do Monte, *J. Phys. Chem. A*, 2019, **123**(10), 1953–1961.
50 E. Ventura and S. A. do Monte, *Theor. Chem. Acc.*, 2020, **139**, 49–57.
51 W. V. E. Doering and L. H. Knox, *J. Am. Chem. Soc.*, 1954, **76**(12), 3203–3206.
52 G. Naville, H. Strauss and E. Heilbronner, *Helv. Chim. Acta*, 1960, **43**, 1221–1243.
53 W. Merk and R. Pettit, *J. Am. Chem. Soc.*, 1968, **90**(3), 814–816.
54 R. E. Harmon, R. Suder and S. K. Gupta, *J. Chem. Soc., Perkin Trans. 1*, 1972, 1746–1749.
55 M. Pomerantz, G. L. Combs, Jr and R. Fink, *J. Org. Chem.*, 1980, **45**, 143–149.
56 M. Pomerantz and G.-S. Swei, *Tetrahedron Lett.*, 1982, **23**, 3027–3030.
57 A. Nagy, J. Fulara and J. P. Maier, *J. Am. Chem. Soc.*, 2011, **133**, 19796–19806.
58 M. J. S. Dewar and C. R. Ganelli, *J. Chem. Soc.*, 1959, 3139–3144.
59 M. L. Cano, M. N. Chrétien and H. García, *Chem. Phys. Lett.*, 2001, **345**, 409–414.
60 A. Hjelmencrantz, A. Friberg and U. Berg, *J. Chem. Soc., Perkin Trans. 2*, 2000, 1293–1300.
61 Y. Zhao, N. E. Schultz and D. G. Truhlar, *J. Chem. Theory Comput.*, 2006, **2**, 364–382.
62 E. I. Izgorodina, U. L. Bernard and D. R. MacFarlane, *J. Phys. Chem. A*, 2009, **113**, 7064–7072.
63 V. Barone and M. Cossi, *J. Phys. Chem. A*, 1998, **102**, 1995–2001.
64 M. Cossi, N. Rega, G. Scalmani and V. Barone, *J. Comput. Chem.*, 2003, **24**, 669–681.
65 S. F. Boys and F. Bernardi, *Mol. Phys.*, 1970, **19**(4), 553–566.
66 S. Simon, M. Duran and J. J. Dannenberg, *J. Chem. Phys.*, 1996, **105**, 11024–11031.
67 R. Ditchfield, D. P. Miller and J. A. Pople, *J. Chem. Phys.*, 1971, **54**, 4186–4193.
68 M. M. Francl, W. J. Pietro, W. J. Hehre, J. S. Binkley, M. S. Gordon and D. J. DeFrees, *J. Chem. Phys.*, 1982, **77**, 3654–3665.
69 W. J. Hehre, R. Ditchfield and J. A. Pople, *J. Chem. Phys.*, 1972, **56**, 2257–2261.
70 P. C. Hariharan and J. A. Pople, *Theor. Chim. Acta*, 1973, **28**, 213–222.
71 R. Krishnan, J. S. Binkley, R. Seeger and J. A. Pople, *J. Chem. Phys.*, 1980, **72**, 650–654.
72 D. J. DeFrees, J. S. Binkley and A. D. McLean, *J. Chem. Phys.*, 1984, **80**, 3720–3725.
73 M. J. Frisch, G. W. Trucks, H. B. Schlegel, G. E. Scuseria, M. A. Robb, J. R. Cheeseman, G. Scalmani, V. Barone, B. Mennucci, G. A. Petersson, H. Nakatsuji, M. Caricato, X. Li, H. P. Hratchian, A. F. Izmaylov, J. Bloino, G. Zheng, J. L. Sonnenberg, M. Hada, M. Ehara, K. Toyota, R. Fukuda, J. Hasegawa, M. Ishida, T. Nakajima, Y. Honda, O. Kitao, H. Nakai, T. Vreven, J. A. Montgomery, Jr, J. E. Peralta, F. Ogliaro, M. Bearpark, J. J. Heyd, E. Brothers, K. N. Kudin, V. N. Staroverov, R. Kobayashi, J. Normand, K. Raghavachari, A. Rendell, J. C. Burant, S. S. Iyengar, J. Tomasi, M. Cossi, N. Rega, J. M. Millam, M. Klene, J. E. Knox, J. B. Cross, V. Bakken, C. Adamo, J. Jaramillo, R. Gomperts, R. E. Stratmann, O. Yazyev, A. J. Austin, R. Cammi, C. Pomelli, J. W. Ochterski, R. L. Martin, K. Morokuma, V. G. Zakrzewski, G. A. Voth, P. Salvador, J. J. Dannenberg, S. Dapprich, A. D. Daniels, Ö. Farkas, J. B. Foresman, J. V. Ortiz, J. Cioslowski and D. J. Fox, *Gaussian 09 Revision D.01*, Gaussian Inc., Wallingford, CT, 2013.
74 T. Yanai, D. P. Tew and N. C. Handy, *Chem. Phys. Lett.*, 2004, **393**, 51–57.
75 M. J. G. Peach, P. Benfield, T. Helgaker and D. J. Tozer, *J. Chem. Phys.*, 2008, **128**, 044118–044125.
76 Z.-L. Cai, M. J. Crossley, J. R. Reimers, R. Kobayashi and R. D. Amos, *J. Phys. Chem. B*, 2006, **110**, 15624–15632.
77 R. Kobayashi and R. D. Amos, *Chem. Phys. Lett.*, 2006, **420**, 106–109.
78 J. Aragó, J. C. Sancho-García, E. Ortí and D. Beljonne, *J. Chem. Theory Comput.*, 2011, **7**, 2068–2077.

79 C.-H. Shu, S.-Z. Zhang, C.-X. Wang, J.-L. Chen, Y. He, K.-J. Shi and P.-N. Liu, *Chem. Commun.*, 2018, **54**, 13670–13676.
80 T. Koenig and J. C. Chang, *J. Am. Chem. Soc.*, 1978, **100**, 2240–2242.
81 C. E. Check, T. O. Faust, J. M. Bailey, B. J. Wright, T. M. Gilbert and L. S. Sunderlin, *J. Phys. Chem. A*, 2001, **105**, 8111–8116.
82 A. G. Harrison, L. R. Honnen, H. J. Dauben, Jr and F. P. Lossin, *J. Am. Chem. Soc.*, 1960, **82**, 5593–5598.
83 J. Yarwood, *Spectroscopy and Structure of Molecular Complexes*, Springer Science + Business Media, New York, 1973, p. 235.
84 J. Joseph and E. D. Jemmis, *J. Am. Chem. Soc.*, 2007, **129**, 4620–4632.
85 E. A. Gislason, *Alkali Halide Vapors. Structure, Spectra, and Reaction Dynamics*, ed. P. Davidovits and D. L. McFadden, Academic Press, New York, 1979, ch. 13.
86 K.-C. Lin and A. G. Ureña, *Int. Rev. Phys. Chem.*, 2007, **26**, 289–352.
87 P. R. Brooks, *Mol. Phys.*, 2012, **110**, 1729–1738.
88 R. W. Anderson and D. R. Herschbach, *J. Chem. Phys.*, 1975, **62**, 2666–2677.
89 H. S. Carman, P. W. Harland and P. R. Brooks, *J. Phys. Chem.*, 1986, **90**, 944–948.
90 H. J. Loesch and J. Möller, *J. Phys. Chem. A*, 1997, **101**, 7534–7543.
91 P. R. Brooks, *J. Vac. Soc. Jpn.*, 2010, **53**, 635–644.
92 E. A. Gislason and J. G. Sachs, *J. Chem. Phys.*, 1975, **62**, 2678–2689.
93 S. Yang and A. M. Ellis, *Chem. Soc. Rev.*, 2013, **42**, 472–484.
94 J. P. Toennies and A. F. Vilesov, *Angew. Chem., Int. Ed.*, 2004, **43**, 2622–2648.
95 A. Mauracher, O. Echt, A. M. Ellis, S. Yang, D. K. Bohme, J. Postler, A. Kaiser, S. Denifl and P. Scheier, *Phys. Rep.*, 2018, **751**, 1–90.
96 P. R. Franke, J. T. Brice, C. P. Moradi, H. F. Schaeffer III and G. E. Douberly, *J. Phys. Chem. A*, 2019, **123**, 3558–3568.
97 G. P. Moradi, A. M. Morrison, S. J. Klippenstein, C. F. Goldsmith and G. E. Douberly, *J. Phys. Chem. A*, 2013, **117**, 13626–13635.
98 A. M. Morrison, J. Agarwal, H. F. Schaefer, III and G. E. Douberly, *J. Phys. Chem. A*, 2012, **116**, 5299–5304.
99 J. M. Merritt, J. Küpperw and R. E. Miller, *Phys. Chem. Chem. Phys.*, 2007, **9**, 401–416.
100 C. P. Moradi and G. E. Douberly, *J. Phys. Chem. A*, 2015, **119**, 12028–12035.
101 G. E. Douberly and R. E. Miller, *J. Phys. Chem. B*, 2003, **107**, 4500–4507.
102 S. Rudić, J. M. Merritt and R. E. Miller, *J. Chem. Phys.*, 2006, **124**, 104305–104312.
103 J. M. Merritt, G. E. Douberly, P. L. Stiles and R. E. Miller, *J. Phys. Chem. A*, 2007, **111**, 12304–12316.
104 T. Liang and G. E. Douberly, *Chem. Phys. Lett.*, 2012, **551**, 54–59.
105 M. Y. Choi, G. E. Douberly, T. M. Falconer, W. K. Lewis, C. M. Lindsay, J. M. Merritt, P. L. Stiles and R. E. Miller, *Int. Rev. Phys. Chem.*, 2006, **25**(1–2), 15–75.
106 C. P. Moradi, C. Xie, M. Kaufmann, H. Guo and G. E. Douberly, *J. Chem. Phys.*, 2016, **144**, 164301–164308.
107 D. Mani, T. Fischer, R. Schwan, A. Dey, B. Redlich, A. F. G. Van der Meer, G. Schwaab and M. Havenith, *RSC Adv.*, 2017, **7**, 54318–54325.
108 M. Hartmann, R. E. Miller, J. P. Toennies and A. Vilesov, *Phys. Rev. Lett.*, 1995, **75**, 1566–1569.
109 D. M. Brink and S. Stringari, *Z. Phys. D: At., Mol. Clusters*, 1990, **15**, 257–263.
110 S. A. Krasnokutski and F. Huisken, *J. Phys. Chem. A*, 2011, **115**, 7120–7126.